ADVANCED FUNCTIONAL MATERIALS
www.afm-journal.de



# A Green and Facile Way to Prepare Granadilla-Like Silicon-Based Anode Materials for Li-Ion Batteries

*Lei Zhang, Ranjusha Rajagopalan, Haipeng Guo, Xianluo Hu, Shixue Dou,* and Huakun Liu**

**A yolk-shell-structured carbon@void@silicon (CVS) anode material in which a void space is created between the inside silicon nanoparticle and the outer carbon shell is considered as a promising candidate for Li-ion cells. Untill now, all the previous yolk-shell composites were fabricated through a templating method, wherein the $SiO_2$ layer acts as a sacrificial layer and creates a void by a selective etching method using toxic hydrofluoric acid. However, this method is complex and toxic. Here, a green and facile synthesis of granadilla-like outer carbon coating encapsulated silicon/carbon microspheres which are composed of interconnected carbon framework supported CVS nanobeads is reported. The silicon granadillas are prepared via a modified templating method in which calcium carbonate was selected as a sacrificial layer and acetylene as a carbon precursor. Therefore, the void space inside and among these CVS nanobeads can be formed by removing $CaCO_3$ with diluted hydrochloric acid. As prepared, silicon granadillas having 30% silicon content deliver a reversible capacity of around 1100 mAh $g^{-1}$ at a current density of 250 mA $g^{-1}$ after 200 cycles. Besides, this composite exhibits an excellent rate performance of about 830 and 700 mAh $g^{-1}$ at the current densities of 1000 and 2000 mA $g^{-1}$, respectively.**

## 1. Introduction

Silicon has attracted remarkable attention as a lithium-ion battery anode due to its unparalleled theoretical capacity (≈4200 mAh $g^{-1}$), relatively low discharge potential (≈0.5V vs $Li/Li^+$), abundance, and environmental benignity.[1–6] However, the dramatic volume change (>300%) during lithiation and delithiation processes leads to severe pulverization and continual formation of solid electrolyte interphase (SEI) on the newly formed silicon surfaces, resulting in a large capacity loss.[7–11] Therefore, the cycling performance of silicon-based anodes is still far from satisfactory from a commercial point of view.[12]

Silicon nanoparticles (Si NPs) have been found to tolerate extreme changes in volume with cycling.[13] Hence, great efforts have been made to improve the cycling stability and electrical conductivity by using various Si-based nanostructures, including Si nanowires,[3,14,15] porous Si,[16–19] and conductive agent coated Si such as carbon,[18,20,21] Ag,[22,23] and conducting polymer.[24] Among them, a yolk-shell-structured carbon@void@silicon (CVS) composite[25,26] is quite promising for practical applications, because the void space between the outer carbon shell and the inside Si NP allows the room for volume changes of Si NP without deforming the carbon shell and SEI film, which in turn allows for the growth of a stable SEI on the surface of the outer carbon shell.[26] Besides, the homogeneous carbon coating shell can prevent the electrolyte ingress and the direct contact of Si NPs with the electrolyte, so the SEI will only be formed on the outer surface of the carbon shell, leading to the high Coulombic efficiency and improved cycling stability.[25] For instance, Cui and co-workers achieved a high capacity of ≈2800 mAh $g^{-1}$ with a very good cycling stability (1000 cycles with 74% capacity retention) based on the yolk-shell-structured CVS nanobeads through a templating method. In order to improve the tap density and limit the SEI formation of these CVS nanoparticles, inspired by the structure of a pomegranate fruit they developed a novel secondary structure of silicon anode which composed of the previous CVS nanobeads. However, in the effort to design the void space inside CVS nanobeads, typically, a $SiO_2$ sacrificial layer was first produced by hydrolysis of tetraethyl orthosilicate (TEOS),[25,26] followed with carbon coating and selective etching of $SiO_2$ using hydrofluoric acid (HF). Here, the method to produce $SiO_2$ was expensive and complex. Moreover, HF solution as an etching agent to remove $SiO_2$ is not environmental friendly.

Dr. L. Zhang, Dr. R. Rajagopalan, Dr. H. Guo
Institute for Superconducting and Electronic Materials
University of Wollongong
Wollongong NSW 2522, Australia
Prof. X. Hu
State Key Laboratory of Materials Processing and Die and Mould Technology
School of Materials Science and Engineering
Huazhong University of Science and Technology
Wuhan 430074, P. R. China
Prof. S. Dou
Institute for Superconducting and Electronic Materials
University of Wollongong
Wollongong, NSW 2522, Australia
E-mail: shi@uow.edu.au
Prof. H. Liu
Institute for Superconducting and Electronic Materials
University of Wollongong
Wollongong NSW 2522, Australia
E-mail: hua@uow.edu.au

DOI: 10.1002/adfm.201503777

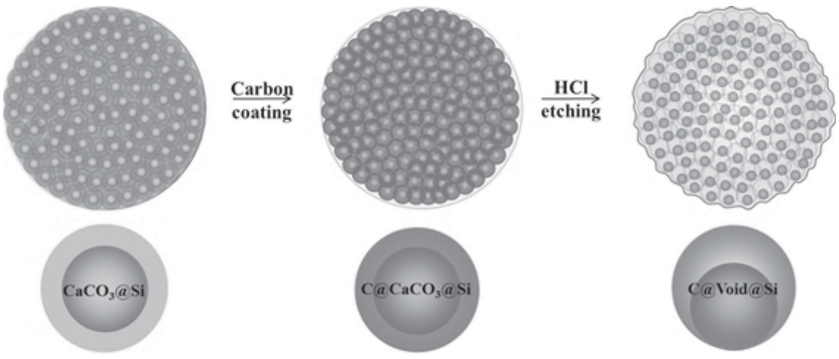


**Figure 1.** Schematic representation of the silicon granadillas composite design.

Considering this fact, new less expensive and environmentally benign methods to prepare yolk-shell silicon anodes are highly desirable.

Here, we report a facile and green method to prepare granadilla-like silicon microspheres. This new approach inherits the advantages of the yolk-shell structure and can be easily scaled up. **Figure 1** illustrates the synthesis procedure of silicon granadillas. We controllably synthesized calcium carbonate@silicon ($CaCO_3$@Si) microspheres in a controlled manner, wherein the Si NPs are individually encapsulated by the $CaCO_3$ framework, followed by carbon deposition and removal of carbonate templates by washing in a dilute hydrochloric acid (HCl). The prepared silicon granadillas coated with the integrated carbon layers on the outer surface (outer shell) are composed of the interconnected porous carbon network supported yolk-shell CVS nanobeads with the Si NP core and the conductive amorphous carbon shell (inside shell), resulting in a unique double-carbon-shell structure. Different from the previous reports in which the $SiO_2$ sacrificial layers coated Si NPs ($SiO_2$@Si) were first fabricated and then the microsized secondary spheres which composed of primary $SiO_2$@Si nanoparticles were prepared via an extra step,[26] $CaCO_3$@Si microspheres were generated through a one-step method within 5 min and showed good spherical morphology. Carbon coating layers were produced via a facile chemical vapor deposition (CVD) method in which acetylene was selected as carbon precursor. Due to the good permeation of acetylene, a homogeneous carbon coating layer could be fabricated not only on the outer surface of the whole silicon granadillas but also the inside every single $CaCO_3$@Si nanobead. This double-carbon-shell structure can effectively prevent electrolyte ingress and improve the electronic conductivity.[26] In addition, different from the previous reports about the CVS nanobeads in which one carbon shell contains more than one Si NP inside, one Si NP was individually encapsulated by one self-supporting hollow carbon sphere in these new CVS, leading to good aggregation free dispersion of Si NPs. Most importantly, in the present study, we first report the carbonate-based templates for the fabrication of the yolk-shell silicon-based anode. Compared with the previous work, this method is much more facile and environment friendly because of the use of diluted HCl instead of HF to remove $CaCO_3$ templates. After HCl treatment, the void space inside and among the CVS nanobeads can be formed, which can better accommodate the huge volume change of Si NPs during the cycling processes.[27]

## 2. Results and Discussion

**Figure 2** shows the SEM images of all the samples. Before carbon coating, all the samples exhibited good spherical morphology. With the increase of silicon content, the size was increased from 3 to 4 μm for 30-$CaCO_3$@Si (Figure 2a), and 4–5 μm for 40-$CaCO_3$@Si (Figure 2b) to 5–6 μm for 50-$CaCO_3$@Si (Figure 2c). During the coprecipitation reaction, the silicon particles play a role in the nucleation, so higher silicon content may result in more reaction inside one carbonate coated silicon microsphere, leading to the increased size of these microspheres. The inset shows the higher magnification images of the single microsphere of 30, 40, and 50-$CaCO_3$ @Si, respectively. It can be seen, that all the Si NPs were well encapsulated by the $CaCO_3$ framework, and a smooth $CaCO_3$ coating layer was generated on the outer surface of the $CaCO_3$@Si microsphere. After carbon coating at high temperature, the obtained

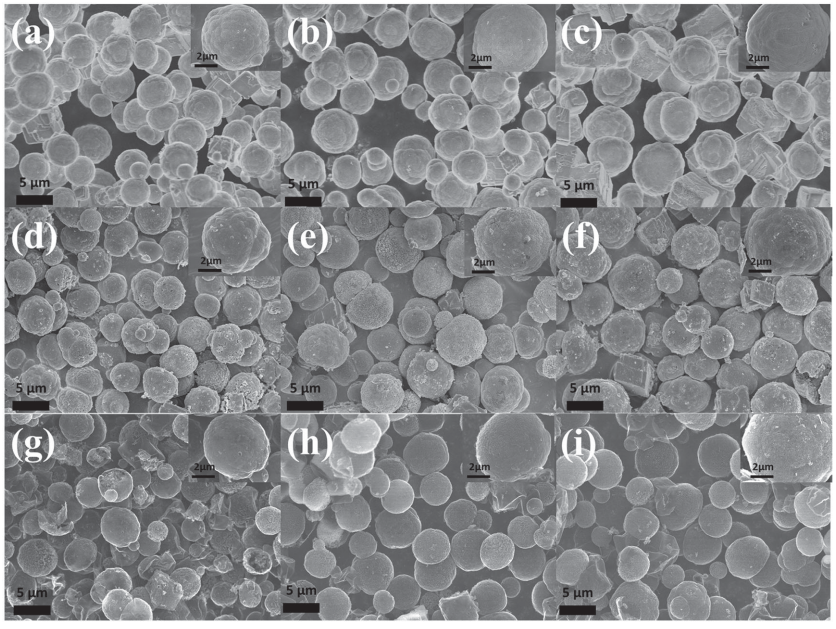


**Figure 2.** SEM images of a) 30-$CaCO_3$@Si, b) 40-$CaCO_3$@Si, c) 50-$CaCO_3$@Si, d) 30-C@$CaCO_3$@Si, e) 40-C@$CaCO_3$@Si, f) 50-C@$CaCO_3$@Si, g) 30@Si-granadillas, h) 40@Si-granadillas, and i) 50@Si-granadillas (the insets show magnified images of the individual microspheres).

30-C@$CaCO_3$@Si (Figure 2d), 40-C@$CaCO_3$@Si (Figure 2e), and 50-C@$CaCO_3$@Si (Figure 2f) retained similar spherical structures and became smoother on the outer surface due to the carbon coating. More importantly, the morphologies of the 30@Si-granadillas (Figure 2g), 40@Si-granadillas (Figure 2h), and 50@Si-granadillas (Figure 2i) were still well maintained after selectively removing the $CaCO_3$ sacrificial layer via HCl treatment. The enlarged single sphere of 30@Si-granadillas in Figure S1 (Supporting Information) clearly shows that all the translucent CVS nanobeads were well coated by the thin and homogeneous outer carbon coatings and supported by a well-connected 3D carbon network.

Transmission electron microscopy (TEM) images of 30, 40, and 50@Si-granadillas are shown in **Figure 3**. For 30@Si-granadillas (Figure 3a), 40@Si-granadillas (Figure 3b) and 50@Si-granadillas (Figure 3c), after HCl treatment, all the interconnected CVS nanobeads with an intact outer carbon shell and the inside Si NP core were well encapsulated by the micronsized outer carbon coating layers, leading to a double-carbon-shell structure. The carbon shell in micrometer-size pouches was coated on the outer surface of the whole silicon granadilla and showed crumpled but homogeneous structure after HCl treatment. In addition, every single Si NP was individually encapsulated by one self-supporting carbon hollow sphere, with well-defined void space between the Si NP core and carbon shell, leading to a good dispersion and aggregation resistant of Si NPs.[25,26] The nanosized CVS nanobeads are uniformly dispersed not only on the surface but also inside the porous carbon framework, which means that the $CaCO_3$@Si microspheres were completely permeated inside the acetylene during the CVD process. This can be confirmed by TME and EDS elemental mapping images in Figure S2a–f in the Supporting Information. According to the EDS in Figure S2j in the Supporting Information, the C, O, and Si can be found in this sample, which correspond to the sample (Cu peaks arise from the specimen holder). Statistical analysis of the volume of the outer carbon hollow sphere ($V_1$) and the inside Si NP ($V_2$) for the CVS nanobeads from 30, 40, and 50@Si-granadillas shows that the average $V_1/V_2$ was centered at 4.25 for 30@Si-granadillas, 3.65 for 40@Si-granadillas, and 2.82 for 50@Si-granadillas (as shown in Figure 3e). The Si NPs utilized for this study have an average diameter of around 80 nm. Assuming a 300%–400% volume expansion of crystalline silicon upon complete lithiation,[25,29] we can see, the void space created in 30 and 40@Si-granadillas are more suitable.[26] After etching away silicon using NaOH, the porous carbon framework was obtained (Figure 3f) and the double-carbon-shell structure was clearly visible. It is seen that this porous carbon microsphere with homogeneous outer carbon shells exhibits good spherical morphology and assembled with interconnected hollow carbon spheres creating a 3D carbon network. Although

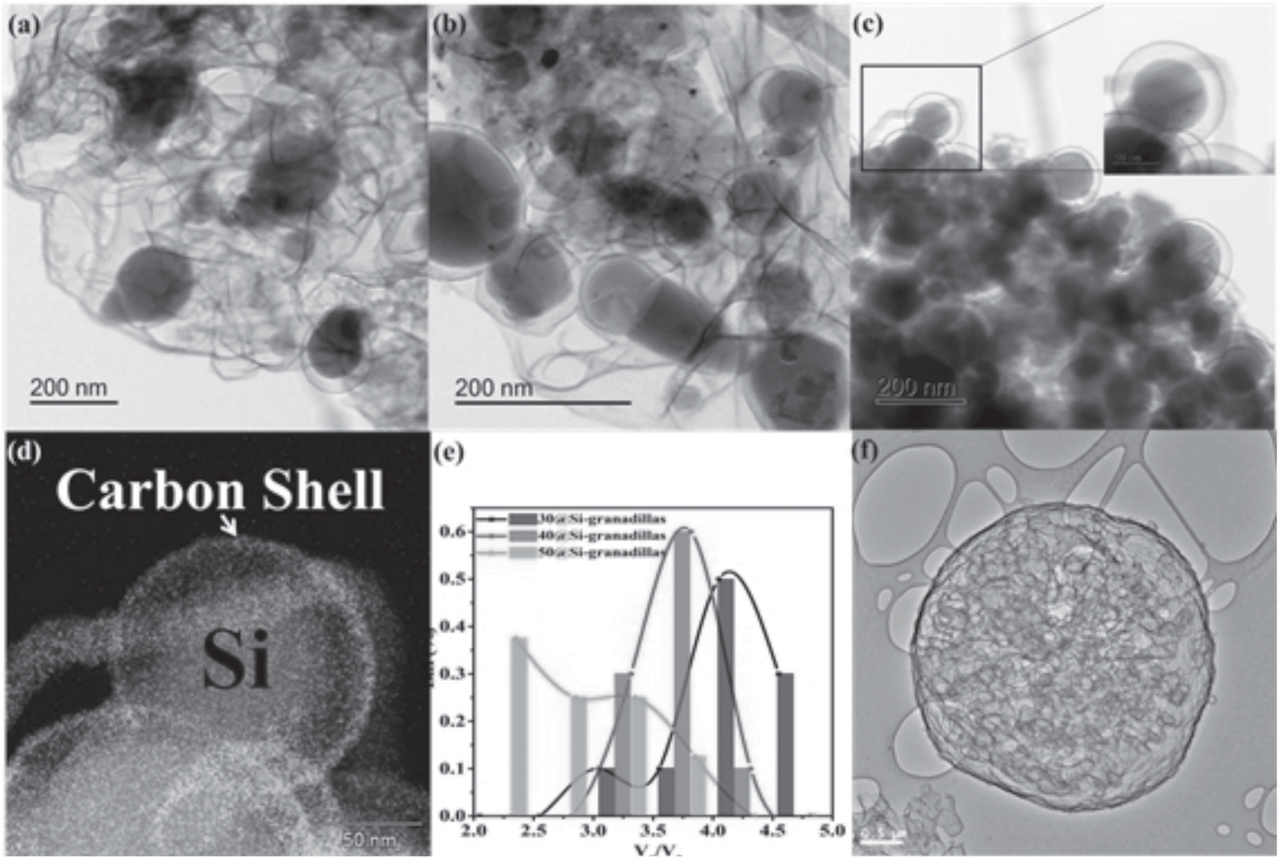


**Figure 3.** TEM images of a) 30@Si-granadillas, b) 40@Si-granadillas, c) 50@Si-granadillas (inset is its high magnification image), d) the EDS elemental mapping of the enlarged CVS from 50@Si-granadillas, carbon (yellow) and silicon (red), e) the statistical analysis of $V_1/V_2$, and f) TEM image of the carbon framework after etching away silicon using NaOH.

the outer carbon shell is only a few nanometers thick, it can still firmly support the whole microbead even after HCl and NaOH etching. This unique double-carbon-shell structure, can provide better protection from the electrolyte, even if the carbon shell inside the CVS nanobeads was broken during cycling, the outer shell can also act as an electrolyte barrier and accommodate the expansion/contraction of the encapsulated Si NPs.[28] Overall, the unique double-carbon-shell structure can provide a better conducting framework, strengthen the mechanical properties, and can also act as an electrolyte blocking layer, so SEI formed mostly outside the silicon granadillas.[26] Besides, the void space inside and among the CVS nanobeads can effectively accommodate the volume expansion of the silicon without rupturing the carbon shell or changing the silicon granadilla size.[26]

**Figure 4**a shows the X-ray diffraction (XRD) patterns of all the samples. For all the samples, there are three distinct diffraction peaks at 2$\theta$ values of 28.3, 47.0, and 55.8°, which can be assigned to (111), (220), and (311) planes of Si phase (JCPDS NO. 27-1402), respectively.[8] Besides the Si phase, the peak at about 25.0° can be assigned to the (002) plane of carbon (JCPDS No. 65-6212).[30] All the (002) peaks are very weaker and broader, indicating the low graphitic crystallinity in these three samples.[31] Figure 4b shows their Raman spectra. The strong peaks at around 500 $cm^{-1}$ for all the samples are ascribed to Si and SiO.[32,33] The weak peak at about 1350 $cm^{-1}$ (D-band) is associated with the amorphous carbon materials,[34] while the strong peak at around 1590.0 $cm^{-1}$ (G-band) is attributed to the vibration of $sp^2$-bonded carbon atoms in a 2D hexagonal lattice,[35] namely the stretching modes of C=C bonds in typical graphite. The low-intensity and weak G-band peak suggests a structural imperfection of the graphene sheets such as defects and small crystal domain size,[36–38] implying these samples have low graphitization degrees. The components of 30, 40 and 50@Si-granadillas were further confirmed by X-ray photoelectron spectra (XPS) spectrum in Figure 4c. The peaks located at 101.1 eV can be assigned to Si 2p, indicating the presence of a layer of silicon oxide species on the surface of all the samples.[32] Strong peaks at 285.2 eV are ascribed to the C 1s.[32] Figure 4d shows the TG curves of 30, 40, and 50@Si-granadillas in air. It can be seen that the weight loss derived from carbon combustion is located in the range of 450–650 °C. The low combustion temperature of silicon granadillas stems from the introduction of carbon with amorphous structure. The residual mass of 30, 40, and 50@Si-granadillas at 700 °C is about 15, 20, and 30 wt%, respectively, suggesting the relevant Si ($SiO_x$) contents in them. In addition, there is a

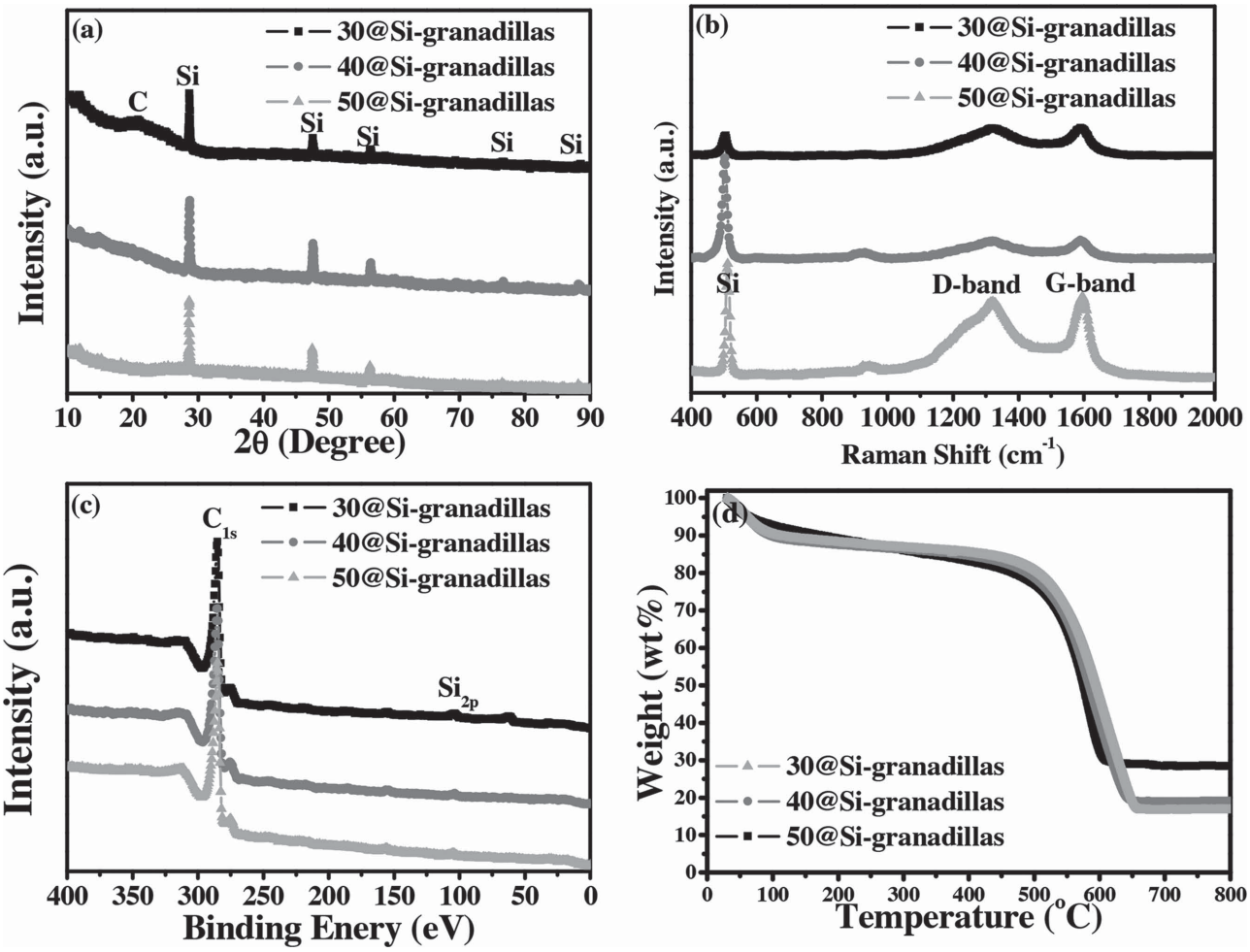


**Figure 4.** a) XRD pattern, b) Raman spectra, c) XPS spectra, and d) TG curves of 30, 40, and 50@Si-granadillas in air.

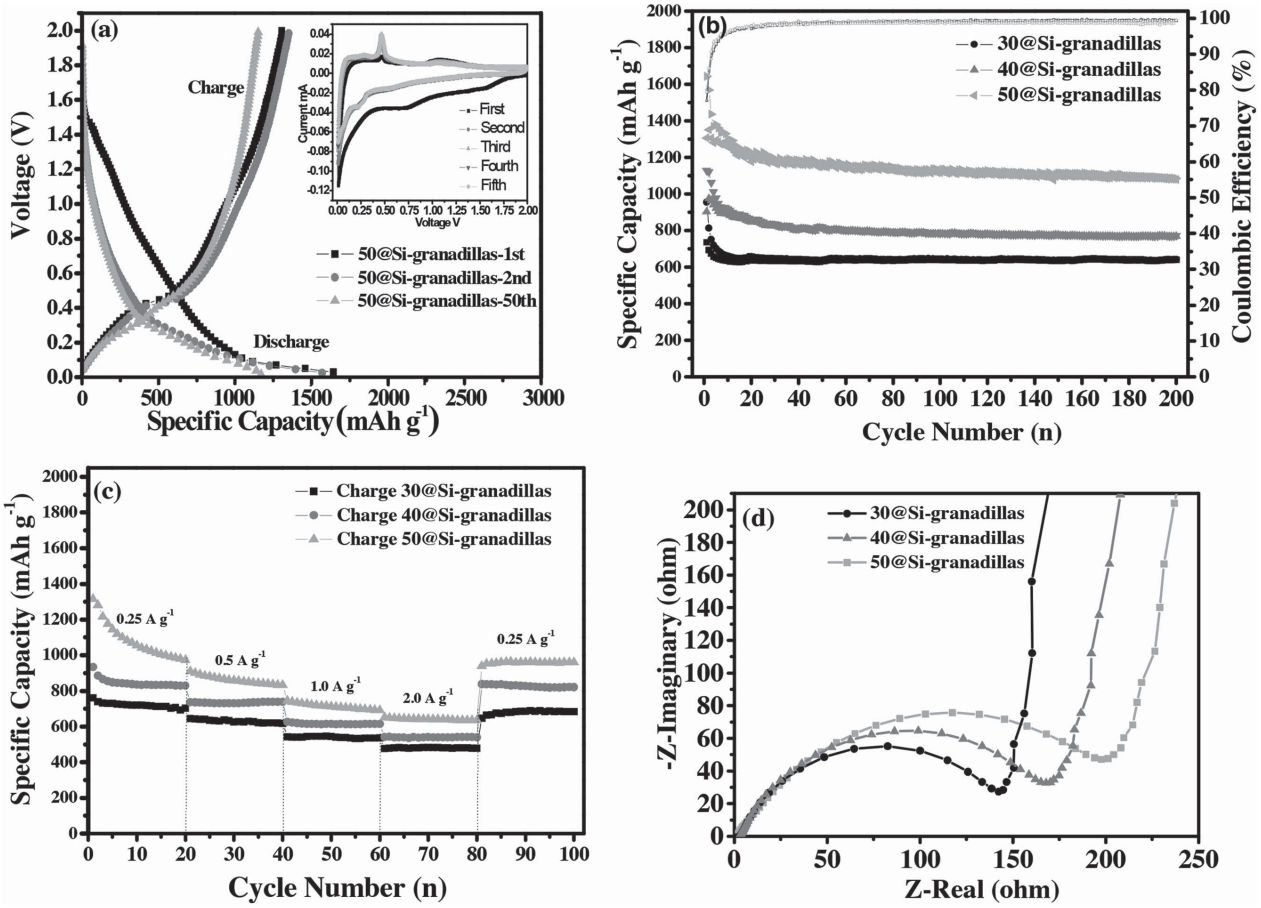


**Figure 5.** Electrochemical properties: a) the discharge–charge curves of 50@Si-granadillas (inset shows the first five CV profiles of 50@Si-granadillas), b) the cycling property, c) the rate performance, and d) the electrochemical impedance plots of 30@Si-granadillas, 40@Si-granadillas, and 50@Si-granadillas anodes

slight weight increase after 700 °C, which means the oxidation of silicon under high temperature.

**Figure 5**a shows the first, second, and fiftieth charge and discharge curves of 50@Si-granadillas at a current density of 250 mA $g^{-1}$. The discharge and charge capacities in the first run are about 1643.9 and 1306.9 mAh $g^{-1}$, thus its initial Coulombic efficiency is 80%. During the first discharge process, sloping voltage plateaus which disappeared in the last cycles between 1.5 and 0.2 V reveals the formation of the stable SEI films on the surface of the electrode, which was further confirmed by the reductive peak in the first cycle of the inserted CV plots in Figure 5a.[39,40] After that, there are long and flat voltage plateaus below 0.2 V which are consistent with the reductive peaks below 0.2 V in the CV plots, suggesting the insertion of lithium ions in carbon and silicon.[41] In addition, voltage plateaus located at about 0.5 V during the charge processes were well maintained even after 50 cycles in 50@Si-granadillas and 200 cycles in 30@Si-granadillas (Figure S3a, Supporting Information) and 40@Si-granadillas (Figure S3b, Supporting Information), which means the extraction of lithium ions from carbon and dealloying of $Li_{4.4}Si$ and consistent with the oxidative peaks at 0.5 V in the CV plots. Compared with the first charge curves of 30@Si-granadillas and 40@Si-granadillas, this plateau showed in 50@Si-granadillas is more obvious because of its higher silicon content.

The cycling performance in Figure 5b shows that the charge capacities of 30@Si-granadillas, 40@Si-granadillas, and 50@Si-granadillas between 2 and 0.01 V at the current density of 250 mA $g^{-1}$ is around 735.0, 903.3, and 1306.9 mAh $g^{-1}$ at the first cycle, and 639.6, 768.8, and 1080.1 mAh $g^{-1}$ after 200 cycles, respectively. As a result, the capacity retention of these samples is about 87.0%, 85.1%, and 82.6% after 200 cycles, suggesting 30@Si-granadillas and 40@Si-granadillas have better cycling stability than that of 50@Si-granadillas. It is known that the theoretical capacity of amorphous carbon is around 600.0 mAh $g^{-1}$.[42] Therefore, the theoretical capacity of 30@Si-granadillas, 40@Si-granadillas, and 50@Si-granadillas are calculated to be around 1140.0, 1320.0, and 1680.0 mAh $g^{-1}$ (based on the TG data). Figure 5c shows the rate performance of the samples at different current densities. The charge capacity of 30@Si-granadillas, 40@Si-granadillas, and 50@Si-granadillas at the first 250 mA $g^{-1}$ after 20 cycles are 703.6, 828.7, and 973.6 mAh $g^{-1}$, respectively, and the retention of the capacity at 500, 1000, and 2000 mA $g^{-1}$ after 20 cycles is 87.8%, 76.3%, and 68.0% for 30@Si-granadillas, 89.1%, 74.1%, and 65.1% for 40@Si-granadillas, and 85.6%, 71.1%, and 65.3% for 50@Si-granadillas, respectively. In addition, the charge–discharge curves of 30@Si-granadillas at the first cycle under different current rates are shown in

Figure S3c in the Supporting Information. It can be seen, even after the big current density cycling test, the plateaus of silicon around 0.5 V can still well maintained. Compared with 50@Si-granadillas, 30@Si-granadillas, and 40@Si-granadillas show the better cycling stability and rate performance. However, 40@Si-granadillas has a higher specific capacity than 30@Si-granadillas due to its higher silicon content. Therefore, based on the point of commercial application, we believe that 40@Si-granadillas is the optimized one among these three samples. Therefore, in order to further check the electrochemical performance of 40@Si-granadillas, the discharge capacity of 40@Si-granadillas at higher current densities between 2 and 0.01 V was tested. In Figure S3d in the Supporting Information, we can see that even we increased the current density to 5 and 10 A $g^{-1}$ and extended the test to 500 cycles, 40@Si-granadillas still maintained a good stability. Besides, the TEM picture of 40@Si-granadillas after fully discharge and SEM pictures of 40@Si-granadillas after 200 cycles were provided in Figure S4 in the Supporting Information to check the integrity of this yolk-shell structure. In Figure S4a (Supporting Information) after the discharge process the volume of silicon particles were increased and they almost fully occupied the inside hollow space without damage the outer carbon coating layer, which means the void we created inside this yolk-shell structure is appropriate. In Figure S4b,c (Supporting Information) good structural integrity can be found for the 40@Si-granadillas after 200 cycles test, which means not only the structure of the inside carbon shell from the yolk-shell nanoparticles but also the outer microsized carbon coating layers were not destroyed.

Figure 5d shows the electrochemical impedance plots of the samples. Although the slopes of their straight lines are very similar, the sizes of their semicircles are different, following a sequence of 50@Si-granadillas < 40@Si-granadillas < 30@Si-granadillas, suggesting that among all the prepared silicon granadillas, 30@Si-granadillas has the lowest resistance to the lithium-ion transfer and the highest electronic conductivity because of the higher carbon content.

Therefore, the silicon granadillas with a silicon content 20 wt% created here show excellent electrochemical properties with the large reversible capacity, good cycling stability, and rate capability. This is because of their unique architecture: 1) the introduction of the interconnected carbon network inside the silicon granadillas and the unique double-carbon-shell structure can effectively strengthen the mechanical properties, improve the electrical conductivity, and prevent the electrolyte ingress;[37,43–46] 2) the developed porous carbon supported yolk-shell structure can provide additional storage sites for lithium ions,[47] better absorb the huge volume change of silicon during cycling, and prevent the aggregation of Si NPs;[25,48,49] 3) the homogenous microspherical morphology leads to less tortuosity of electrode and higher electrolyte diffusion, thus enhancing the rate performance.[50–56]

## 3. Conclusion

In summary, we have demonstrated a facile and scalable method for preparing silicon granadillas anode materials. Silicon granadillas with a homogeneous micronsized carbon shell on the outer surface are composed of a kind of well-connected carbon network supported yolk-shell nanobeads containing Si NPs individually protected by a thin, self-supporting, and conductive hollow carbon shell, leading to a unique double-carbon-shell structure. Rationally designed robust 3D carbon framework, interconnected yolk-shell carbon/silicon nanobeads, and the unique double-carbon-shell endow these silicon granadillas with excellent electrochemical performance. Clearly, the simplicity and scalability of this fabrication process will make silicon granadillas anode material promising for the practical application in the next generation Li-ion cells.

## 4. Experimental Section

### 4.1. Material Synthesis

*Synthesis of $CaCO_3$@Si microspheres*: All the reagents used in the present study were obtained from Sigma Aldrich. $CaCO_3$@Si composites were prepared by means of a coprecipitation process. Stoichiometric amount of sodium carbonate ($Na_2CO_3$) was dissolved in 100 mL deionized (DI) water, and then after vigorously stirred for 2 min, 30 mg silicon (≈80 nm) was added to the above solution under stirring condition. The dispersion was further stirred for another 30 min to get a uniform suspension (a). At same time, solution (b) was prepared by dissolving calcium chloride ($CaCl_2$) in 100 mL DI water. Then, suspension (a) was dropped into solution (b) with vigorous stirring for 5 min to obtain 30-$CaCO_3$@Si suspension which were collected by centrifugation, and washed three times using DI water. For a comparison, 40-$CaCO_3$@Si and 50-$CaCO_3$@Si were fabricated under the same conditions as described above except that 40 and 50 mg silicon was added, respectively.

*Carbon coating on $CaCO_3$@Si composites (C@$CaCO_3$@Si)*: Briefly, the obtained $CaCO_3$@Si was placed in a horizontal quartz tube in a furnace. The tube was firstly purged with purified Ar flow (50 mL $min^{-1}$) for 30 min and then heated to 600 °C at a heating rate of 10 °C $min^{-1}$. Subsequently, acetylene was introduced into the tube at the same temperature with a flow rate of 30 mL $min^{-1}$, and kept at these conditions for 30 min. Finally the system was cooled to room temperature under Ar atmosphere and the sample collected was denoted as 30, 40, or 50-C@$CaCO_3$@Si, respectively.

*$CaCO_3$ layer etching*: $CaCO_3$ sacrificial layer was removed with diluted HCl solution. C@$CaCO_3$@Si powders were immersed in diluted HCl aqueous solution for 30 min, followed by centrifugation and ethanol washing three times. The final silicon granadillas (30, 40, or 50@Si-granadillas) were obtained after drying in a vacuum oven.

### 4.2. Characterization

The products 30, 40, or 50@Si-granadillas were analyzed by XRD; GBC MMA with Cu K$\alpha$ radiation; Raman spectroscopy (JobinYvon HR800) employing a 10 mW helium/neon laser at 632.8 nm; field emission scanning electron microscopy (FESEM; JEOL 7500); and TEM; JEOL ARM-200F with high-resolution TEM (HRTEM). Thermogravimetric analysis (TGA) was performed by using a SETARAM thermogravimetric analyzer (France) in air to determine the changes in sample weight with increasing temperature and to estimate the amount of carbon in the sample. XPS analysis experiment was carried out using Al K$\alpha$ radiation and fixed analyzer transmission mode. The pass energy was 60 eV for the survey spectra and 20 eV for specific elements.

### 4.3. Electrochemical Measurement

The tests were conducted by assembling coin-type half cells in an argon-filled glove box. Lithium foil was employed as both reference and counter electrode. The working electrode consisted of 70 wt% active material (30, 40, or 50@Si-granadillas, respectively), 20 wt% black carbon, and

10 wt% carboxymethyl cellulose (CMC) binder. The electrolyte was 1.0 M LiPF6 in a 1:1 (v/v) mixture of ethylene carbonate (EC) and diethyl carbonate (DEC). Electrochemical cycling of electrodes was conducted at 250 mA $g^{-1}$ for galvanostatic measurements in the 10 mV to 2.0 V (vs $Li/Li^+$) voltage window. Cyclic voltammetry was performed using a Biologic VMP-3 electrochemical workstation between 0.01 and 2.0 V at a scan rate of 0.1 mV $s^{-1}$.

## Supporting Information

Supporting Information is available from the Wiley Online Library or from the author.

## Acknowledgements

This work was supported by a Baosteel-Australia Joint Research and Development Centre (BAJC; Project BA14006), an Auto CRC 2020 (Project 1-117), and the National High-tech R&D Program of China (863 Program, Grant No. 2015AA034601). L.Z. would like to thank CSC scholarships from China. The authors would also like to thank Dr. Tania Silver for critical reading of the manuscript and Dr. Dongqi Shi for XPS testing and the authors also acknowledge the use of the facilities in the UOW Electron Microscopy Center, with particular thanks to Dr. Gilberto Casillas-Garcia.

Received: September 6, 2015
Revised: October 22, 2015
Published online: December 9, 2015

[1] I. Kovalenko, B. Zdyrko, A. Magasinski, B. Hertzberg, Z. Milicev, R. Burtovyy, I. Luzinov, G. Yushin, *Science* **2011**, *334*, 75.
[2] M. Armand, J.-M. Tarascon, *Nature* **2008**, *451*, 652.
[3] A. M. Chockla, J. T. Harris, V. A. Akhavan, T. D. Bogart, V. C. Holmberg, C. Steinhagen, C. B. Mullins, K. J. Stevenson, B. A. Korgel, *J. Am. Chem. Soc.* **2011**, *133*, 20914.
[4] B. Liu, X. Wang, H. Chen, Z. Wang, D. Chen, Y. B. Cheng, C. Zhou, G. Shen, *Sci. Rep.* **2013**, *3*, 1622.
[5] X. Zhou, Y.-X. Yin, A.-M. Cao, L.-J. Wan, Y.-G. Guo, *ACS Appl. Mater. Interfaces* **2012**, *4*, 2824.
[6] H. Jia, P. Gao, J. Yang, J. Wang, Y. Nuli, Z. Yang, *Adv. Energy Mater.* **2011**, *1*, 1036.
[7] X. L. Bin Wang, Xianfeng Zhang, Bin Luo, Meihua Jin, Minghui Liang, Shadi A. Dayeh, S. T. Picraux, Linjie Zhi, *ACS Nano* **2013**, *7*, 1437.
[8] J. Yu, H. H. Zhan, Y. H. Wang, Z. L. I. Zhang, H. Chen, H. Li, Z. Y. Zhong, F. B. Su, *J. Power Sources* **2013**, *228*, 112.
[9] P. Gu, R. Cai, Y. Zhou, Z. Shao, *Electrochim. Acta* **2010**, *55*, 3876.
[10] W. Wang, P. N. Kumta, *ACS Nano* **2010**, *4*, 2233.
[11] X. H. Liu, L. Zhong, S. Huang, S. X. Mao, T. Zhu, J. Y. Huang, *ACS Nano* **2012**, *6*, 1522.
[12] J. Z. Xianghong, Liu Wenping, Si Lixia Xi, Barbara Eichler, Chenglin Yan, Oliver G. Schmidt, *ACS Nano* **2015**, *9*, 1198.
[13] Y. G. Guo, J. S. Hu, L. J. Wan, *Adv. Mater.* **2008**, *20*, 2878.
[14] A. Kohandehghan, P. Kalisvaart, K. Cui, M. Kupsta, E. Memarzadeh, D. Mitlin, *J. Mater. Chem. A* **2013**, *1*, 12850.
[15] T. Song, J. Xia, J. H. Lee, D. H. Lee, M. S. Kwon, J. M. Choi, J. Wu, S. K. Doo, H. Chang, W. I. Park, D. S. Zang, H. Kim, Y. Huang, K. C. Hwang, J. A. Rogers, U. Paik, *Nano Lett.* **2010**, *10*, 1710.
[16] Z. Zhang, Y. Wang, W. Ren, Q. Tan, Z. Zhong, F. Su, *Adv. Electron. Mater.* **2015**, *1*, 1400059.
[17] M. Y. Ge, J. P. Rong, X. Fang, A. Y. Zhang, Y. H. Lu, C. W. Zhou, *Nano Res.* **2013**, *6*, 174.
[18] Z. Zhang, Y. Wang, W. Ren, Q. Tan, Y. Chen, H. Li, Z. Zhong, F. Su, *Angew. Chem. Int. Ed.* **2014**, *53*, 5165.
[19] X. Huang, J. Yang, S. Mao, J. Chang, P. B. Hallac, C. R. Fell, B. Metz, J. Jiang, P. T. Hurley, J. Chen, *Adv. Mater.* **2014**, *26*, 4326.
[20] J. H. Kong, W. A. Yee, Y. F. Wei, L. P. Yang, J. M. Ang, S. L. Phua, S. Y. Wong, R. Zhou, Y. L. Dong, X. Li, X. H. Lu, *Nanoscale* **2013**, *5*, 2967.
[21] J. Yu, H. Zhan, Y. Wang, Z. Zhang, H. Chen, H. Li, Z. Zhong, F. Su, *J. Power Sources* **2013**, *228*, 112.
[22] F.-H. Du, K.-X. Wang, W. Fu, P.-F. Gao, J.-F. Wang, J. Yang, J.-S. Chen, *J. Mater. Chem. A* **2013**, *1*, 13648.
[23] Y. Yu, L. Gu, C. Zhu, S. Tsukimoto, P. A. van Aken, J. Maier, *Adv. Mater.* **2010**, *22*, 2247.
[24] B. Liu, P. Soares, C. Checkles, Y. Zhao, G. Yu, *Nano Lett.* **2013**, *13*, 3414.
[25] N. Liu, H. Wu, M. T. McDowell, Y. Yao, C. Wang, Y. Cui, *Nano Lett.* **2012**, *12*, 3315.
[26] N. Liu, Z. Lu, J. Zhao, M. T. McDowell, H. W. Lee, W. Zhao, Y. Cui, *Nat. Nanotechnol.* **2014**, *9*, 187.
[27] D. S. Jung, T. H. Hwang, S. B. Park, J. W. Choi, *Nano Lett.* **2013**, *13*, 2092.
[28] J. Luo, X. Zhao, J. Wu, H. D. Jang, H. H. Kung, J. Huang, *J. Phys. Chem. Lett.* **2012**, *3*, 1824.
[29] L. Xue, G. Xu, Y. Li, S. Li, K. Fu, Q. Shi, X. Zhang, *ACS Appl. Mater. Interfaces* **2012**, *5*, 21.
[30] Y. Wang, F. Su, C. D. Wood, J. Y. Lee, X. S. Zhao, *Ind. Eng. Chem. Res.* **2008**, *47*, 2294.
[31] K. Fu, L. Xue, O. Yildiz, S. Li, H. Lee, Y. Li, G. Xu, L. Zhou, P. D. Bradford, X. Zhang, *Nano Energy* **2013**, *2*, 976.
[32] X. Zhu, H. Chen, Y. Wang, L. Xia, Q. Tan, H. Li, Z. Zhong, F. Su, X. Zhao, *J. Mater. Chem. A* **2013**, *1*, 4483.
[33] J. I. Lee, K. T. Lee, J. Cho, J. Kim, N. S. Choi, S. Park, *Angew. Chem.* **2012**, *124*, 2821.
[34] S. Ray, C. Pao, H. Tsai, B. Bose, J. Chiou, W. Pong, D. DasGupta, *Carbon* **2006**, *44*, 1982.
[35] L. Ji, X. Zhang, *Carbon* **2009**, *47*, 3219.
[36] F. Su, X. Zhao, Y. Wang, J. Zeng, Z. Zhou, J. Y. Lee, *J. Phys. Chem. B* **2005**, *109*, 20200.
[37] A. Cuesta, P. Dhamelincourt, J. Laureyns, A. Martinez-Alonso, J. M. Tascón, *J. Mater. Chem.* **1998**, *8*, 2875.
[38] Q. Yang, W. Xu, A. Tomita, T. Kyotani, *J. Am. Chem. Soc.* **2005**, *127*, 8956.
[39] E. Buiel, J. Dahn, *Electrochim. Acta* **1999**, *45*, 121.
[40] H. Fujimoto, A. Mabuchi, K. Tokumitsu, T. Kasuh, *J. Power Sources* **1995**, *54*, 440.
[41] A. Magasinski, P. Dixon, B. Hertzberg, A. Kvit, J. Ayala, G. Yushin, *Nat. Mater.* **2010**, *9*, 353.
[42] L. Zhang, M. Zhang, Y. Wang, Z. Zhang, G. Kan, C. Wang, Z. Zhong, F. Su, *J. Mater. Chem. A* **2014**, *2*, 10161.
[43] J. Hu, H. Li, X. Huang, *Solid State Ionics* **2007**, *178*, 265.
[44] J. Hu, H. Li, X. Huang, *Solid State Ionics* **2005**, *176*, 1151.
[45] Q. Wang, H. Li, L. Chen, X. Huang, *Carbon* **2001**, *39*, 2211.
[46] Q. Wang, H. Li, L. Chen, X. Huang, *Solid State Ionics* **2002**, *152*, 43.
[47] F. Zhang, K.-X. Wang, G.-D. Li, J.-S. Chen, *Electrochem. Commun.* **2009**, *11*, 130.
[48] A. Vu, Y. Qian, A. Stein, *Adv. Energy Mater.* **2012**, *2*, 1056.
[49] T. Cetinkaya, M. Uysal, M. O. Guler, H. Akbulut, A. Alp, *Powder Technol.* **2014**, *253*, 63.
[50] M. Ebner, D.-W. Chung, R. E. García, V. Wood, *Adv. Energy Mater.* **2014**, *4*, 1301278.
[51] J. Liu, P. Kopold, P. A. van Aken, J. Maier, Y. Yu, *Angew. Chem. Int. Ed.* **2015**, *54*, 9632.
[52] Y. Yu, L. Gu, C. B. Zhu, S. Tsukimoto, P. A. van Aken, J. Maier, *Adv. Mater.* **2010**, *22*, 2247.
[53] N. Mahmood, J. Zhu, S. Rehman, Q. Li, Y. Hou, *Nano Energy* **2015**, *15*, 755.
[54] Q. Li, N. Mahmood, J. H. Zhu, Y. L. Hou, S. H. Sun, *Nano Today* **2014**, *9*, 668.
[55] N. Mahmood, C. Zhang, F. Liu, J. Zhu, Y. Hou, *ACS Nano* **2013**, *9*, 10307.
[56] C. Zhang, N. Mahmood, H. Yin, F. Liu, Y. Hou, *Adv. Mater.* **2013**, *25*, 4932.